Northumbria Research Link

Citation: Lawgaly, Ashref and Khelifi, Fouad (2017) Sensor Pattern Noise Estimation Based on Improved Locally Adaptive DCT Filtering and Weighted Averaging for Source Camera Identification and Verification. IEEE Transactions on Information Forensics and Security, 12 (2). pp. 392-404. ISSN 1556-6013

Published by: IEEE

URL: https://doi.org/10.1109/TIFS.2016.2620280 <https://doi.org/10.1109/TIFS.2016.2620280>

This version was downloaded from Northumbria Research Link: http://nrl.northumbria.ac.uk/id/eprint/28227/

Northumbria University has developed Northumbria Research Link (NRL) to enable users to access the University's research output. Copyright © and moral rights for items on NRL are retained by the individual author(s) and/or other copyright owners. Single copies of full items can be reproduced, displayed or performed, and given to third parties in any format or medium for personal research or study, educational, or not-for-profit purposes without prior permission or charge, provided the authors, title and full bibliographic details are given, as well as a hyperlink and/or URL to the original metadata page. The content must not be changed in any way. Full items must not be sold commercially in any format or medium without formal permission of the copyright holder. The full policy is available online: http://nrl.northumbria.ac.uk/policies.html

This document may differ from the final, published version of the research and has been made available online in accordance with publisher policies. To read and/or cite from the published version of the research, please visit the publisher's website (a subscription may be required.)

Northumbria University NEWCASTLE

University Library

Sensor Pattern Noise Estimation Based on Improved Locally Adaptive DCT Filtering and Weighted Averaging for Source Camera Identification and Verification

Ashref Lawgaly, and Fouad Khelifi, *Member, IEEE*

***Abstract*—Photo Response Non-Uniformity (PRNU) noise is a sensor pattern noise characterizing the imaging device. It has been broadly used in the literature for source camera identification and image authentication. The abundant information that the sensor pattern noise carries in terms of the frequency content makes it unique, and hence suitable for identifying the source camera and detecting image forgeries. However, the PRNU extraction process is inevitably faced with the presence of image-dependent information as well as other non-unique noise components. To reduce such undesirable effects, researchers have developed a number of techniques in different stages of the process, i.e., the filtering stage, the estimation stage, and the post-estimation stage. In this paper, we present a new PRNU-based source camera identification and verification system and propose enhancements in different stages. First, an improved version of the Locally Adaptive Discrete Cosine Transform (LADCT) filter is proposed in the filtering stage. In the estimation stage, a new Weighted Averaging (WA) technique is presented. The post-estimation stage consists of concatenating the PRNUs estimated from color planes in order to exploit the presence of physical PRNU components in different channels. Experimental results on two image datasets acquired by various camera devices have shown a significant gain obtained with the proposed enhancements in each stage as well as the superiority of the overall system over related state-of-the-art systems.**

***Index Terms*—Photo Response Non-Uniformity noise, Source Camera Identification, digital image forensics.**

I. Introduction

OVER the last decade, the use of digital image devices has incredibly become widespread due to the advance of digital technologies. Nowadays, every digital multimedia device incorporates a camera for taking good quality pictures at no cost. As a result, digital pictures constitute a reliable means for testifying incidents and providing legally acceptable evidence in courtroom. However, a digital picture can be edited, transmitted and distributed easily with recent technologies such as Bluetooth and Internet. Therefore, knowing the source of the image and verifying its integrity is essential in forensic applications. The field of image forensics is concerned with authentication, integrity verification and Source Camera Identification (SCI) [1]. Over the last decade, a significant number of attempts to extract features which characterize the camera device have been reported in the literature [1]–[27]. Fig. 1 shows the common process to produce a picture via a digital imaging device. A digital device fingerprint could be characterizing some of the following components; the Color Filter Array (CFA) interpolation artifacts [2], [3], the lens aberration noise [4], [5], sensor dust [6], Photo Response Non-Uniformity(PRNU) noise [7]–[27].

Ashref Lawgaly and Fouad Khelifi are with the Department of Computer Science and Digital Technologies, Northumbria University, UK. (e-mail: ashref.lawgaly@northumbria.ac.uk; fouad.khelifi@northumbria.ac.uk).

This work addresses the problem of source camera identification and verification in image forensics based on PRNU estimation. It is worth mentioning that the PRNU is the result of imperfections caused by the manufacturing process due to the lack of homogeneity of the silicon area in the imaging sensor [28]. The noise due to sensor imperfections is a weak signal of the same size as the output image denoted here by $K \in \Re^{\omega \times \nu}$, where $\omega \times \nu$ represent the dimension of the sensor. Regardless of the sensor type, the final camera output is expressed as [8] [10]

$$I = I^0 + I^0 K + \Theta \tag{1}$$

where I^0 is the original input image. $I^0 K$ represents the PRNU term and Θ is a random noise factor respectively. Note that the effect of the sensor pattern noise K on the original image follows a multiplicative rule. It has been reported in the literature that the PRNU is very similar to a white Gaussian noise and hence abundant in terms of the frequency content and unique to every sensor allowing for reliable identification even if the camera devices under investigation are of the same brand and model. This also enables the investigator to verify the authenticity of digital images and detect forgeries.

In the literature, there has been a growing body of research devoted to source camera identification using the PRNU. The PRNU estimation process can be divided into three stages, i.e., the filtering stage, the estimation stage, and finally the post-estimation (enhancement) stage. In the filtering stage, a pattern residual signal, also called the noise residue is obtained from each image through the difference between the input image and its filtered version.

$$r = I - F(I) \tag{2}$$

where r is the noise residue containing the PRNU and $F(\cdot)$ is the filtering process. In the estimation stage, the PRNU is estimated from a set of noise residues. In the post-estimation stage, the PRNU is enhanced further for better camera identifi-

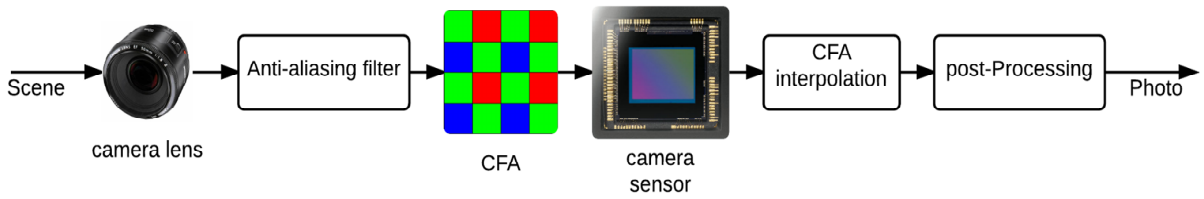

Fig. 1. Image acquisition process for an ordinary digital camera.

cation. The most widely known system was initially developed by Lukas *et al*. [7] [8] in order to identify the origin of digital images using the PRNU. It uses a set of images to extract a noise residue from each image. The estimated noise residues are then averaged to obtain a camera reference PRNU noise. In [9] [10], the Maximum Likelihood Estimator (MLE) was applied to estimate the camera reference PRNU. In [10], the authors proposed preprocessing steps to enhance the commonly used PRNU through Wiener filtering and zero-mean operations. The rational is that there are artefacts which may be shared by different cameras of the same model or brand and this leads to a rise in false identification rates. In [11], the authors noticed that the estimated PRNU with a commonly used technique [8] does not have the characteristics of white Gaussian noise. They proposed to whiten the noise residues by using only the phase component in the Fourier domain. The author in [12] pointed out that the PRNU obtained from an image may be contaminated by its content especially if it is characterized by edges, contours, and texture. His idea is based on the assumption that the less trustworthy components are the stronger signals components in a PRNU, and therefore they should be attenuated. Nevertheless, attenuating strong components from a signal may lead to reduction of the useful PRNU components too [11]. In [13], an image sharpening idea is used to amplify the high frequency content of PRNU noise in images. This process can ensure a strong presence of PRNU before estimation. In [14], the authors proposed an improved technique based on the assumption that the large element of the PRNU is more trustworthy and consequently should be utilized in the matching stage, while other elements are discarded. Another technique has been proposed in [15] for suppressing the random noise contamination in the PRNU noise. The aim of this approach is achieved by clustering the PRNU pixels of similar values, the pixels of PRNU are sorted a descending/ascending order. Next, every number of pixels is averaged and the positions of the clustered pixels are saved, in order to be applied noise residue of the tested image. Theoretically, such process could generate a higher quality reduced-size PRNU, which may lead to a more trustworthy PRNU than its original full-size one. In [16] an approach based on a Weighted Averaging (WA) technique to optimize PRNU estimation was applied. The idea is based on the assumption that images are acquired under different conditions making the corresponding residual signals different from each other. For instance, bright images provide better sensor pattern noise estimation than dark images. Also, saturated pixels cause undesirable noise in residual signals. In this approach the steps of removing undesirable components are applied as proposed in [10]. In [17], the Principal Component Analysis (PCA) method was used to reduce the dimensionality of the PRNU noise and attenuate the effect of scene details on the filtering process. The idea underlying this algorithm is that the energy of the noise residuals characterizing the reference PRNU is concentrated in a small subspace of the entire eigenspace, while the remaining energy represents undesirable (image-dependent) noise components. Therefore, by preserving only the most important subspace (characterized by the eigenvectors which are associated to the most significant eigenvalues) and then conducting the inverse PCA transform, the image-dependent noise could be significantly attenuated. In [18], the authors showed that the use of random projections can significantly reduce the dimension of fingerprints without affecting the camera identification performance. The authors adopted a compressive sensing method to represent the sensor fingerprints space by a dictionary.

Since the filtering stage contributes significantly to the accuracy of PRNU estimation, the influence of denoising filter has been discussed in [29] for forgery detection and [30] for source camera identification. The authors show that the Block-matching and 3D filtering (BM3D) algorithm [31] outperforms the wavelet-based Mihcak's filter [32] which was initially adopted in [8]. In [33], it has been shown that the accuracy of sensor pattern noise estimation can also be improved by removing the denoising distortions. In [19], the author pointed out that although the wavelet-based Mihcak's filter has been commonly accepted in the literature for estimating the noise residue, it may spread the details and edges of an image creating various disturbing signals around such areas. This leads to a decrease in correlation between the noise residue and the right PRNU. He introduced a PRNU estimation technique using a combination of adaptive Wiener and median filtering in the pixel domain. This suggested filtering approach is followed by an enhancement strategy where only the pixels with high probabilities of significant noise residue bias are retained. Kang *et al*. [20] developed a filter based on an eight-neighbor context-adaptive interpolation algorithm. In this technique the local regions are classified into six types: vertically edged, horizontally edged, smooth, right-diagonal edge, left-diagonal edge and others. The method can estimate the center-pixel values in different local regions since it is adaptive to local image context. Consequently, the difference between the actual values and the predicted ones could reduce the effect of the edges while PRNU components are preserved.

Other attempts focused on color combination to exploit the presence of the PRNU in different color planes. Indeed, the authors in [21] proposed a color decoupling algorithm prior

to the filtering stage to reduce the color interpolation noise which is caused by the CFA. In [22], three color combination schemes were proposed to obtain the final PRNU using the red, green and blue channels. The basic idea is to extract the PRNU from each color channel separately and then select the pixel with the largest magnitude. Furthermore, the similarity between the estimated PRNU and the noise residue is another parameter which may affect the performance of the source camera identification system. Initially, researchers adopted the normalized correlation as in [7]–[10] and [12]–[19]. Then, with the aim of reducing the effect of periodic noise contamination and hence enhancing the false positive rate in SCI, the peak to correlation energy (PCE) was proposed [23] [34]. The main idea behind PCE is to consider the correlation between the PRNU and shifted versions of the noise residue in order to lessen the similarity which may exist between the PRNU of a specific camera and the noise residue of an image taken by a different camera. In [11], the authors used an improved version of PCE called the correlation over circular cross-correlation norm (CCN) by taking into account the negative values of correlation between the PRNU and noise residues estimated from images of different cameras. The CCN has been shown to reduce the false positive rate to half of that with PCE. In [24], a pre-processing technique based on spectrum equalization has been developed to decrease the false identification rate. The idea is to equalize the magnitude spectrum of the PRNU by detecting and suppressing the memorable peaks according to the local characteristics because such peaks in the spectrum are likely to be created by periodic artifacts. More recently, the PRNU has been used to detect forgeries caused by Hue modification [35].

As discussed earlier, the process of source camera identification and/or verification has different stages. In this paper, we present a new PRNU-based source camera identification and verification system and propose enhancements in different stages of the process. First, an improved version of the Locally Adaptive Discrete Cosine Transform (LADCT) filter is proposed in the filtering stage. In the estimation stage, a new weighted averaging technique is presented. The post-estimation stage consists of combining PRNU signals where each is estimated from a color plane in order to exploit the presence of physical PRNU components in different channels. Experimental results on two image datasets, acquired by various camera devices, have shown a significant gain obtained with the proposed enhancements in each stage and the superiority of the overall system over related state-of-the-art systems. The rest of this paper is structured as follows; Section II describes the proposed system and discusses its different components in detail. Experimental results and analysis are provided in Section III. A conclusion is drawn in Section IV.

II. Proposed system

Fig. 2 illustrates the proposed source camera identification system. First, digital images are considered in the form of separate color channels. Then, an improved version of the LADCT de-noising filter is applied to reduce the effect of scene details on noise residues. Next, for efficient sensor pattern noise estimation, the obtained noise residues are averaged using the proposed WA technique. Finally, we propose to concatenate the PRNUs estimated from the primary color planes in order to exploit the presence of physical PRNU components in different color channels. In camera identification, the noise residue of a query image is compared to all PRNUs stored in the database. The closest PRNU corresponds to the camera which has been used to take the image. In camera verification, however, the similarity between the noise residue and the PRNU of a certain camera is compared to a given threshold in order to verify whether the image is originated by the camera. The system's components will be discussed in more detail in the next subsections.

A. Improved Locally Adaptive DCT filter

The Discrete Cosine Transform (DCT) has been broadly adopted in applications of image processing including feature extraction, quality assessment, filtering, and compression [36]. The Locally Adaptive DCT filter (LADCT) has a range of advantages exceeding other filters that operate on full images, such as wavelets and is meant to perform well on images affected by image-dependent noise including the multiplicative noise [37]. This gives a good reason for adopting this filter because the PRNU is also multiplicative. The LADCT filter operates on sliding blocks (local action filter), which could offer more information about the local effect of noise on the image in a better fashion [38]. Furthermore, it performs well on different noise models such as Poisson and film-grain types [39]. Finally, averaging multiple de-noised estimates for each pixel in the block will overcome the problem of undershoots and overshoots which occur around the neighborhood of discontinuities as a result of the Gibbs Phenomenon [40] and this is directly related to the problem of scene details in the estimated sensor pattern noise. The authors in [37] introduced the LADCT filter for a type of noise that contaminates the signal through a multiplicative rule. They used a sliding block window to obtain de-noised estimates of neighboring and overlapping blocks. The multiple estimates are then averaged to suppress artifacts caused by undershoots and overshoots around the highly textured regions. The threshold for each block depends on the local mean of the block and the local noise variance. This filter was referred to as LADCT_1 in [37] and is improved here. Since we are concerned with the extraction of PRNU, which is a multiplicative noise, for source camera identification, we take advantage of the LADCT_1 filter. To the best of our knowledge, this filter has not been used in the field of image forensics. The main steps of LADCT_1 are summarized below.

1) The image is first divided into blocks of $u \times u$ pixels. Let S be a horizontal or vertical shift ($S = 1$) between two consecutive blocks. According to [37], the best performance of the filter can be achieved when $u = 8$ and $S = 1$ (This is why number 1 is included in the notation of LADCT_1).
2) For each block b whose upper left corner is at (m, l),

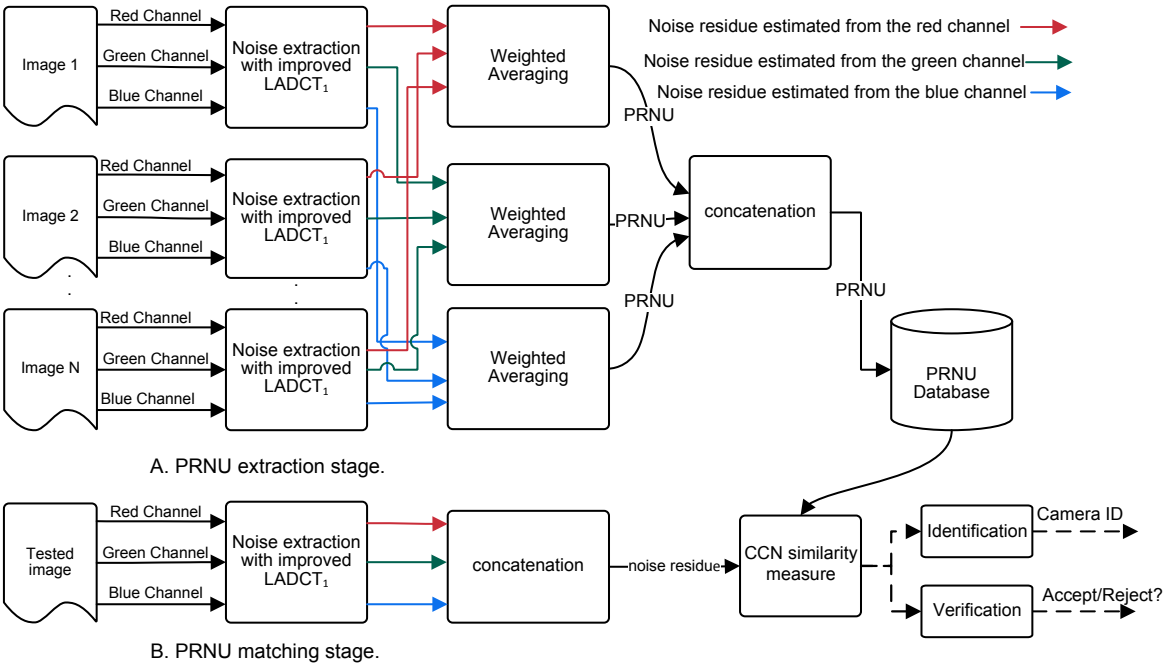

Fig. 2. Proposed source camera identification and verification system.

DCT coefficients are computed as

$$B(p,q) = c(p)\ c(q) \quad \times \sum_{m=0}^{u-1}\sum_{l=0}^{u-1} b(m,l)\cos(\frac{(2m+1)p\pi}{2u})\cos(\frac{(2l+1)q\pi}{2u}) \quad (3)$$

where

$$c(i) = \begin{cases} \sqrt{\frac{2}{u}} & if\ \ 1 \le i \le u-1 \\ \frac{1}{\sqrt{u}} & i = 0 \end{cases}$$

3) A threshold is computed for each block as

$$T = k\ \sigma\ \bar{b} \quad (4)$$

where $k = 2.6$ is a constant which controls the threshold value. $\bar{b}$ refers to the local mean of the block and σ represents the noise standard deviation.

4) Hard thresholding is applied on each DCT coefficient as

$$B'(p,q) = \begin{cases} B(p,q) & if\ \ |B(p,q)| > T \\ 0 & Otherwise \end{cases} \quad (5)$$

where $B'(p,q)$ is the result of thresholding $B(p,q)$.

5) The processed blocks are reconstructed in the pixel domain using the inverse DCT as

$$b'(m,l) = c(p)\ c(q) \quad \times \sum_{p=0}^{u-1}\sum_{q=0}^{u-1} B'(p,q)\cos(\frac{(2m+1)p\pi}{2u})\cos(\frac{(2l+1)q\pi}{2u}) \quad (6)$$

6) The final estimate for a pixel at (m,l) is computed by averaging the multiple estimates at the same location which were obtained from overlapping blocks due to the shifting process.

It is worth mentioning that the conventional LADCT$_1$ filter uses the same threshold on blocks that are characterized with a similar statistical mean regardless of their textural information (see (4)). However, the filtering process inevitably removes a portion of the image content along with the SPN and because natural images are not stationary, it is sensible to set a varying threshold, especially across blocks of small size (8×8), which depends on their textural content that has been removed by the filter. In order to adjust the LADCT$_1$ filter for PRNU estimation, we propose an improved version of the filter in the following.

As illustrated by Fig. 3, we introduce two improvements of LADCT$_1$. The first improvement is based on estimating the noise variance for every block independently using the threshold as described above (Steps 1-6). This is to estimate a block-dependent threshold which will be used in another stage of the LADCT$_1$ filtering. The proposed method for estimating a threshold for each block consists of two phases as follows. Let us define an estimate of the sensor pattern noise K as

$$\widehat{K} = \frac{\sum_{i=1}^{N}(I_i - f(I_i))}{\sum_{i=1}^{N} f(I_i)} \quad (7)$$

where I_i is the i^{th} observed image and $f(I_i)$ represents its filtered version with the conventional LADCT$_1$ where $\sigma^2 = 0.002$. Denote by n_K the estimation noise for K where $\widehat{K} = K + n_K$. In practice, the estimation noise n_K is more significant than the actual K since the correlation between various estimates of $\widehat{k}$ obtained from different sets of images of the same camera is normally very small (i.e. less than 0.2). Given a block b, let us consider only the dominant portion of

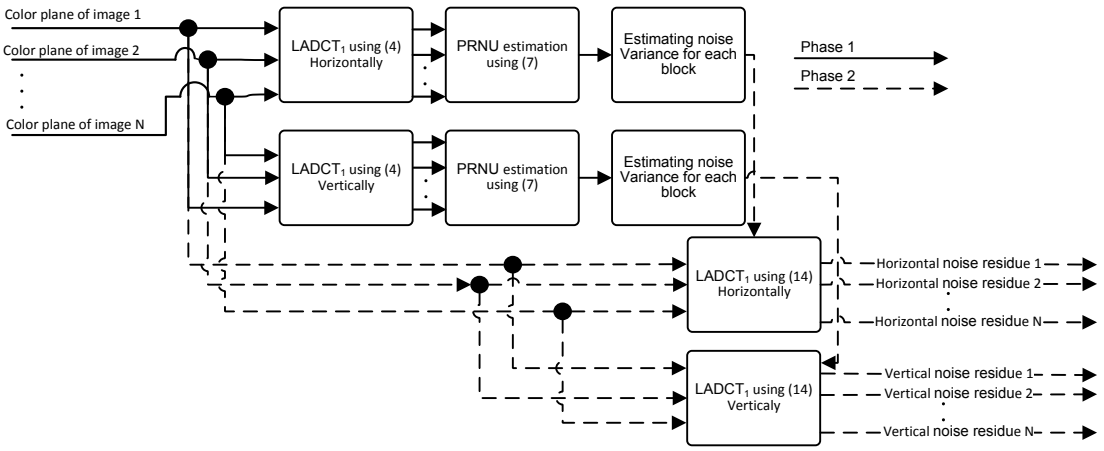

Fig. 3. Extraction of noise residues corresponding to a single color plane for PRNU estimation based on improved LADCT_1.

noise in the model given in (1) as

$$I_b \approx I_b^0 + I_b^0 K_b \tag{8}$$

If $I_b^0 K_b$ is viewed as an additive noise, the block-dependent threshold T_b can be given as [41]

$$T_b = k\ \sigma_b \tag{9}$$

where k is a constant which can be determined empirically (see (4)). σ_b^2 is the additive noise variance which can be expressed approximately as[1]

$$\sigma_b^2 \approx E[b^2]\sigma_{K_b}^2 \tag{10}$$

where $\sigma_{K_b}^2$ represents the variance of K within the block b. It follows

$$T_b = k\ \sqrt{E[b^2]}\ \sigma_{K_b} \tag{11}$$

However, the estimate of $\sigma_{K_b}^2$ cannot be obtained from (7) because of the significance of n_K as mentioned earlier. Indeed,

$$\sigma_{\widehat{K}}^2 = \sigma_K^2 + \sigma_{n_K}^2 \tag{12}$$

and likewise

$$\sigma_{\widehat{K}_b}^2 = \sigma_{K_b}^2 + \sigma_{n_{K_b}}^2 \tag{13}$$

where $\sigma_{n_{K_b}}$ represents the standard deviation of n_K within the block b. To overcome this issue, we instead take into account the local presence of textural image content n_{K_b} in the estimate of $\widehat{K}$ by the conventional filter. The following threshold is proposed for each block b

$$T_b = k\ \sqrt{E[b^2]}\ \sigma\ \frac{\sigma_{\widehat{K}}}{\sigma_{\widehat{K}_b}} \tag{14}$$

where σ is the noise standard deviation as used in (4). The idea underlying this threshold value is based on the fact that the statistical variance of the estimated noise may vary significantly across blocks. Therefore, blocks in which the estimated noise $\widehat{K}_b$ has high variance should be filtered with a relatively small threshold in the DCT domain to retain the image content because the high activity in such blocks is likely to be from edges and texture (i.e. n_{K_b}). On the other hand, a low variance estimate of noise in a block could well represent the actual sensor pattern noise and thus should be filtered out with a relatively large threshold. $\sigma_{\widehat{K}}$ is used in the ratio as a reference to measure the extent to which the estimated noise has high or low activity in a specific block. Finally, the second moment in (14) enables us to exploit bright regions more than dark ones since the multiplicative nature of the sensor pattern noise makes its presence stronger in bright regions. As for the second method of enhancement, it is worth noting that the LADCT_1 filter was initially used [37] in just one direction. This is sensible for image de-noising purposes since the size of the filtered image has to be the same as the original one. In our application, however, we can have two versions of the filtered image and hence two PRNUs each estimated in one direction (horizontal and vertical). The rationale behind this process is to increase the size of the PRNU camera reference and noise residue in order to reduce to probability of false alarms (i.e. reduce the similarity between PRNUs and noise residues of different cameras). Indeed, there could be some components of the PRNU that are hard to estimate in the horizontal direction but estimable in the vertical direction and vice versa. We refer to the combination of the PRNU estimates in the horizontal and vertical directions as LADCT_1^{HV}.

B. Weighted Averaging

The WA technique relies on the principle of unknown signal estimation from noisy observations [42] [43]. As discussed earlier, the PRNU is estimated using N images I_i, $i = 1,\ 2\cdots, N$. Denote by L the number of samples of each image rearranged in one direction (i.e. vertically or horizontally). In view of (1) and (2), the corresponding noise residue can be expressed as

$$\begin{aligned} r_i(j) &\approx I_i^0(j)K(j) + \Phi_i(j) \\ j &= 1,\ 2\cdots, L \end{aligned} \tag{15}$$

where Φ_i is an independent noise. For the sake of demonstration, let us assume that the images used for estimating the PRNU represent smooth regions describing the same color

[1]In (10), the second moment of the observed image block I_b is assumed to be equal to that of the original image block I_b^0.

information such as blue sky content (i.e., the variance of $I_i^0(j)$ is extremely small $\sigma^2_{I_i^0(j)} \ll 1$). This may not be true in practice but the development given below remains valid to some extent as will be shown in experiments on natural images of various content. Let ξ be a constant so that $\xi = \frac{1}{NL}\sum_{i=1}^{N}\sum_{j=1}^{L} I_i^0(j)$. It follows

$$\begin{aligned} r_i(j) &\approx \xi K(j) + \Psi_i(j) \\ &= s(j) + \Psi_i(j) \end{aligned} \tag{16}$$

where $s(j) = \xi K(j)$ and

$$\begin{aligned} \Psi_i(j) &= \Phi_i(j) - K(j)(\xi - I_i^0(j)) \\ &\approx \Phi_i(j) \end{aligned} \tag{17}$$

Here we are mainly interested in the sensor pattern noise K. In view of (16) and (17), the problem of estimating the PRNU from a set of N images can be seen as an estimation of an unknown signal $s(j)$ with $j = 1,\ 2\cdots, L$ in a noisy environment, i.e., using N noisy observations. The i^{th} observation r_i is the sum of a signal s and a random noise Ψ_i with zero mean and a variance for each observation equal to σ_i^2. The conventional method to estimate s consists of averaging the observations [44]

$$\hat{s}(j) = \frac{1}{N}\sum_{i=1}^{N} r_i(j) \tag{18}$$

In the rest of the paper, this technique is referred to as constant averaging because each observation is equally multiplied by the same weight which is a constant factor of 1/N. Most state-of-the-art systems use the idea of constant averaging for estimating the PRNU; this is based on the assumption that each noise residue is a noisy observation of the PRNU because images are acquired under different conditions, making the corresponding noise residues distinct from each other. For example, bright images provide better PRNU estimation than dark images. Also, saturated pixels raise estimation errors in residual signals [8]. However, constant averaging is not optimal if the noise variance σ_i^2 changes from one observation to another. Theoretically speaking, the WA technique offers the closest estimation to the actual signal in terms of the mean squared error [42] [45]. The estimated signal with WA is described as

$$\hat{s}(j) = \sum_{i=1}^{N} w_i r_i(j) \tag{19}$$

where w_i is a weight corresponding to the i^{th} noise residue r_i. The optimal weight for the i^{th} observation is given by (See Appendix A)

$$w_i = \frac{1}{\sigma_i^2}\left(\frac{1}{\sum_{k=1}^{N}\frac{1}{\sigma_k^2}}\right) \tag{20}$$

Obviously, the weights depend on the variance of undesirable noise Ψ_i in each observation. As proposed in [42], the estimated noise variance can be computed as

$$\sigma_i^2 = \frac{\sum_{j=1}^{L}(\hat{n}_i(j) - \bar{n}_i)^2}{L} \tag{21}$$

with

$$\hat{n}_i(j) = r_i(j) - \bar{r}(j) \tag{22}$$

where $\bar{n}_i$ denotes the mean of the estimated noise $\hat{n}_i$ and $\bar{r}(j) = \frac{1}{N}\sum_{i=1}^{N} r_i(j)$ represents the average signal. The estimated PRNU term with WA can be computed as

$$PRNU(j) = \sum_{i=1}^{N} w_i r_i(j) \tag{23}$$

C. Color PRNU concatenation

A challenging task for estimating the PRNU consists of the color channel to take into consideration at each pixel location. This is because of the three primary colors (Red, Green and Blue), the sensor exhibits a physical noise pattern in one color component only at each pixel location, while the other components are estimated through interpolation involving the neighboring pixels [8]. Some PRNU estimation techniques, such as [19], [25], rely on the gray scale version of images to extract the PRNU. Alternatively, the authors in [8], [17], [26] estimated the PRNU from each channel separately and then combined them linearly to derive a color-to-luminance PRNU. The common rule for calculating the Luminance component Y is

$$Y = 0.30\ I_R + 0.59\ I_G + 0.11\ I_B \tag{24}$$

where I_R, I_G, and I_B represent the red, green, and blue channels respectively. Other techniques use only the green channel in order to extract the PRNU as it contains more physical PRNU information when compared to the other channels [11] [27]. However, the linear combination of color channels with fixed weights would include some interpolation noise if a certain color location does not correspond to the physical light information. Indeed, the combination of three PRNU estimates may have an adversary effect on performance because only one estimate corresponds to the actual PRNU component while the two other estimates represent noise. The noise estimates may cancel the actual one due to the linear combination. On the other hand, if the green channel only is used, the physical PRNU information which could exist in other color components (red and blue) is not taken into account. In [22], a non-linear combination is applied by extracting the PRNU from each color channel separately, and then the largest coefficient in magnitude at each location is chosen. In this work, the PRNU is estimated from each channel separately and then the resulting PRNUs are concatenated to form a color PRNU. Similarly, a color noise residue can be obtained from the test image through concatenation of the three noise residues, each corresponding to a color plane. This way the physical information characterizing the PRNU can be exploited efficiently.

D. CCN similarity measure

Finally, the proposed system performs the Circular Correlation Norm (CCN) as proposed in [11] to measure the similarity between the PRNU x and the noise residue y estimated from a query image. For a $\omega \times \nu$ query image, the size of the PRNU

is $\omega' \times \nu'$ where $\omega' = 2\omega$ and $\nu' = 3\nu$. The CCN measure is defined as

$$CCN(x,y) = \frac{\psi_{xy}(0,0)}{\sqrt{\frac{1}{\omega' \times \nu' - |A|} \sum_{m_1,m_2 \notin A} \psi^2_{xy}(m_1,m_2)}} \quad (25)$$

where A is a small neighbor area typically of size 11×11 around the central point at $(0,0)$, $|A|$ is the number of pixels in A, and $\psi_{xy}(m_1,m_2)$ represents the circular cross-correlation expressed as

$$\psi_{xy}(m_1,m_2) = \frac{\sum_{i=0}^{\omega'-1} \sum_{j=0}^{\nu'-1} x(i,j) y(i \oplus m_1, j \oplus m_2)}{\omega' \times \nu'} \quad (26)$$

where $\oplus$ is the modulo addition with $i \oplus m_1 = (i + m_1) \mod \omega'$ and $j \oplus m_2 = (j + m_2) \mod \nu'$.

III. Experimental results

In this section, a number of experiments have been conducted to assess the performance of the proposed system. The evaluation has been conducted using two different datasets; our dataset and the Dresden Dataset [46]. Tables I and II list the cameras used in each dataset with the technical properties of each camera sensor. In this experimental evaluation, each

TABLE I
Digital cameras in our dataset.

Brand	Resolution	Sensor	Images
Canon IXUS115HS-1	4000×3000	1/2.3", CMOS	250
Canon IXUS115HS-2	4000×3000	1/2.3", CMOS	250
Canon G10	4416×3312	1/1.7", CCD	250
Fujifilm S2950-1	4288×3216	1/2.3", CCD	250
Fujifilm S2950-2	4288×3216	1/2.3", CCD	250
Nikon Coolpix L330-1	5152×3864	1/2.3", CCD	250
Nikon Coolpix L330-2	5152×3864	1/2.3", CCD	250
Panasonic DMC TZ20-1	4320×3240	1/2.33", CMOS	250
Panasonic DMC TZ20-2	4320×3240	1/2.33", CMOS	250
Samsung pl120-1	4320×3240	1/2.33", CCD	250
Samsung pl120-2	4320×3240	1/2.33", CCD	250
Samsung L301	4000×3000	1/2.3", CCD	250
Sony DSC HX200V	4896×3672	1/2.3", CMOS	250

TABLE II
Digital cameras in Dresden dataset.

Brand	Resolution	Sensor	Images
AgfaPhoto DC-733s	3072×2304	1/2.5", CCD	281
AgfaPhoto DC-830i	3264×2448	1/1.8", CCD	363
Kodak M1063-0	3664×2748	1/2.33", CCD	464
Kodak M1063-1	3664×2748	1/2.33", CCD	458
Nikon D200-0	3872×2592	372.9 mm^2, CCD	372
Nikon D200-1	3872×2592	372.9 mm^2, CCD	380
Panasonic DMC-FZ50-0	3648×2736	1/1.8", CCD	265
Panasonic DMC-FZ50-1	3648×2736	1/1.8", CCD	415
Sony DSC-H50-0	3456×2592	1/2.33", CCD	284
Sony DSC-H50-1	3456×2592	1/2.33", CCD	257

PRNU is estimated from 50 natural images captured by the same sensor. To measure the effect of the image size on performance, the extraction of PRNU has been carried out by considering cropped blocks from the images with different sizes,i.e., 128×128, 256×256 and 512×512. The blocks are taken from the center of each image without affecting its content.

A. Analysis of the system's components

Since there are three contributions in the proposed system, i.e. improvement of the LADCT$_1$ filter, weighted averaging, and color combination, it is sensible to assess each part separately to highlight the improvements gained at each stage. As mentioned earlier, 50 images have been used to estimate the PRNU while the remaining ones are used as test images. A pattern noise residue is estimated from each test image and compared with the extracted PRNUS. For fair comparison, however, the normal correlation coefficient is used at the matching stage in this section since it was adopted in related competing techniques. This also enables us to measure the gain obtained when the CCN is used, instead, in subsection III-B. In the identification experiments, the False Negative Rate (FNR) and False Positive Rate (FPR) are computed to evaluate the performance. Denote by y_i^j the noise residue of a test image i taken by a camera C^j whose PRNU is x^j. Let $\rho(y_i^j)$ be the closest PRNU to y_i^j according to the similarity measure used. Given M different cameras where N_j is the number of test images per camera C^j, the FNR for the j^{th} camera is defined as

$$FNR(j) = 100 \times Prob(\rho(y_i^j) \neq x^j) \quad i \in \{1,2,\cdots,N_j\} \quad (27)$$

Likewise, the FPR for the j^{th} camera is given by

$$FPR(j) = 100 \times Prob(\rho(y_i^k) = x^j | y_i^k \notin C^j) \quad k \in \{1,2,\cdots,M\} \; ; \; i \in \{1,2,\cdots,N_j\} \quad (28)$$

The overall FNR and FPR given as FNR$= \frac{1}{M} \sum_{j=1}^{M} FNR(j)$ and FPR$= \frac{1}{M} \sum_{j=1}^{M} FPR(j)$, respectively, are used in our identification experiments.

1) Enhanced LADCT$_1$ filtering: In this part, the advantage of the proposed enhancements to the conventional LADCT$_1$ filter for camera identification is demonstrated. The performance LADCT$_1$ and its improved versions are evaluated. Note that the constant averaging is used to obtain the PRNU in this part as we are concerned with the filtering process only. With regards to the conventional LADCT$_1$, the noise variance for each image block is constant. In order to get the optimal parameter setting for LADCT$_1$, we tested different values for the noise variance σ^2 (see (4)). On both datasets, table III shows that the best results can be achieved with a value[2] of $\sigma^2 = 0.002$. Table IV depicts the identification performance obtained when using LADCT$_1$ in two directions, i.e., horizontal and vertical which is referred here to as LADCT$_1^{HV}$ as well as the gain of the proposed enhancement with block-based noise variance (i.e. using (14)). For the sake of comparison, three other filters used in the literature for PRNU estimation have been listed, namely the wavelet-based Mihcak's filter [8], [32], the BM3D filter [31], and the predictive filter based on eight-neighbor context-adaptive interpolation (PCAI8) [20]. It can be seen that the proposed enhancements significantly reduce the FNR and FPR when compared with the conventional

[2]This optimal value ($\sigma^2 = 0.002$) is very likely to be the same on datasets with different cameras. Otherwise, the forensic analyst may create two sub-sets from the available images. One sub-set to estimate the PRNU and another sub-set (i.e., a validation sub-set) to find σ.

TABLE III
OVERALL FNR AND FPR RESULTS IN (%) ON BOTH DATASETS WITH VARIOUS σ^2.

	Our Dataset						Dresden Dataset					
	FNR			FPR			FNR			FPR		
σ^2	128	256	512	128	256	512	128	256	512	128	256	512
0.012	42.38	19.81	9.50	3.53	1.65	0.79	55.80	31.06	12.13	6.20	3.45	1.35
0.007	35.54	16.42	8.81	2.96	1.37	0.73	48.12	24.40	8.31	5.35	2.71	0.92
0.004	32.96	14.77	7.81	2.75	1.24	0.65	41.64	18.99	5.56	4.63	2.11	0.62
0.002	**29.50**	**14.62**	**7.38**	**2.46**	**1.22**	**0.62**	**36.47**	**16.28**	**5.41**	**4.05**	**1.79**	**0.60**
0.001	30.15	14.73	7.42	2.48	1.24	**0.62**	37.00	16.60	**5.41**	4.14	1.85	0.61

TABLE IV
OVERALL FNR AND FPR RESULTS IN (%) ON BOTH DATASETS WITH DIFFERENT FILTERS.

	Our Dataset						Dresden Dataset					
	FNR			FPR			FNR			FPR		
Filter	128	256	512	128	256	512	128	256	512	128	256	512
Wavelet-based [8], [32]	24.96	12.15	7.08	2.10	1.06	0.61	30.48	11.40	2.95	3.37	1.20	0.37
BM3D [31]	27.85	13.00	7.08	2.38	1.04	0.61	34.64	14.65	3.00	3.97	1.55	0.40
PCAI8 [20]	43.58	22.15	9.92	3.47	1.91	0.85	44.93	23.53	6.81	4.92	2.89	0.95
Conventional (i.e. (4))	29.50	14.62	7.38	2.46	1.22	0.62	36.47	16.28	5.41	4.05	1.79	0.60
LADCT_1^H with (14)	27.96	13.58	7.12	2.33	1.13	0.59	33.14	13.77	4.69	3.68	1.53	0.52
LADCT_1^{HV} with (4)	24.85	12.77	6.92	2.07	1.06	0.58	29.71	11.21	3.00	3.30	1.25	0.40
LADCT_1^{HV} with (14)	**23.65**	**12.04**	**6.77**	**1.97**	**1.00**	**0.56**	**25.75**	**9.52**	**2.90**	**2.86**	**1.06**	**0.32**

LADCT_1 filter. With such enhancements, the proposed filter outperforms other competing filters. Interestingly, BM3D and PCAI8 perform worse than the wavelet-based Mihcak's filter. These findings are actually in perfect agreement with those obtained in [24] (page 134, Fig. 5). This can be justified by the fact that, in the original papers [20], [30] where these filters were shown to outperform the wavelet-based Mihcak's filter, blue sky images were used to estimate the PRNU. This suggests that the filters are very sensitive to the content of images used. It is, however, worth noting that the assumption on the availability of blue sky images may not be realistic in practical forensic applications.

Since most of the computational complexity in PRNU estimation is due to the filtering process, the computational cost of the filters is evaluated here. The average running time on a test image of size 512×512 is compared. All the source codes were implemented in MATLAB and run on a platform of an Intel Core Duo i7 $-$ 4770 CPU 3.40GHz with 16 GB of memory. We used the authors' implementation of the wavelet-based Mihcak's filter and BM3D while we implemented the other filters. The results in (*ms*) are depicted in Table V. The computational cost of the proposed filter is low

TABLE V
CPU TIMES OF DIFFERENT FILTERING OPERATIONS.

Filter	CPU Time (*ms*)
BM3D [31]	4344
PCAI8 [20]	3155
Wavelet-based [8], [32]	851
LADCT_1^{HV}	1505

in comparison with PCAI8 and BM3D but is slightly higher than that of the wavelet-based filter. It is, however, worth mentioning that the main computational component in our proposed filter is the DCT and inverse DCT applied on 8×8 image blocks. Therefore, one can explore some parallelism to run these transforms on image blocks of different locations simultaneously since each block DCT (or inverse block DCT) does not depend on the result of other block DCTs (or inverse block DCTs).

2) Weighted averaging vs constant averaging: In the rest of the paper, the improved LADCT_1 filter, i.e., LADCT_1^{HV} with the proposed block-based adaptive threshold as given in (14) is used unless otherwise stated. In this section, the efficiency of the WA technique is illustrated. It is worth noting that only the green channel is used for the PRNU and noise residue estimation in this section. The analysis of color combination methods will be discussed in the next experiment. The results depicted in Table VI show that the WA LADCT_1^{HV} offers a clear improvement over the constant averaging-based PRNU estimation with the LADCT_1^{HV} filter for both datasets. This is true for all image sizes. As can be seen, significant enhancements are obtained especially on the Dresden dataset with image size 128×128 and 256×256, where the decrease in FNR and FPR reaches 15% and 30% respectively. However, smaller improvements have been achieved on our dataset.

3) Color PRNU evaluation: Here we adopt the WA technique discussed earlier. Different methods for combining color channels in PRNU estimation are assessed. That is, the green channel-based PRNU as suggested in [11] [27], the luminance image-based PRNU estimation as mentioned in [19] [25], the luminance PRNU method as proposed in [8] [17] [26], and finally the color combination scheme developed in [22]. Note that the authors in [22] developed three schemes but scheme 3 is used here because it has been found to deliver the best performance. The results shown in Table VII reveal an interesting finding in that the PRNU extracted from gray level images seems to offer better source camera identification than that of the green channel in both datasets. Also, it is clear that the combination of the three RGB channels as proposed in [22] outperforms the methods which use the green channel only, the Luminance image and the luminance PRNU. Finally, the proposed color concatenation achieves the best performance among the tested methods.

TABLE VI
OVERALL FNR AND FPR RESULTS IN (%) ON BOTH DATASETS WITH CONSTANT AND WEIGHTED AVERAGING METHODS.

	Our Dataset						Dresden Dataset					
	FNR			FPR			FNR			FPR		
Averaging	128	256	512	128	256	512	128	256	512	128	256	512
Constant	23.65	12.04	6.77	1.97	1.00	0.56	25.75	9.52	2.90	2.86	1.06	0.32
Weighted	**23.58**	**11.12**	**6.69**	**1.96**	**0.92**	**0.55**	**21.69**	**6.62**	**1.79**	**2.41**	**0.74**	**0.20**

TABLE VII
OVERALL FNR AND FPR RESULTS IN (%) ON BOTH DATASETS WITH DIFFERENT COLOR COMBINATION METHODS.

	Our Dataset						Dresden Dataset					
	FNR			FPR			FNR			FPR		
Method	128	256	512	128	256	512	128	256	512	128	256	512
Green plane [11] [27]	23.58	11.12	6.69	1.96	0.92	0.55	21.69	6.62	1.79	2.41	0.74	0.20
Luminance image [19] [25]	23.35	10.73	6.42	1.95	0.89	0.54	20.10	6.09	1.64	2.23	0.68	0.18
Luminance PRNU [8] [17] [26]	22.46	10.40	6.40	1.87	0.90	**0.52**	19.28	5.60	1.60	2.14	0.60	0.20
RGB scheme 3 [22]	22.46	10.58	6.30	1.87	0.88	**0.52**	18.31	5.41	1.55	2.03	0.60	0.17
Color concatenation	**21.35**	**10.20**	**6.10**	**1.78**	**0.85**	**0.52**	**14.40**	**4.15**	**1.45**	**1.72**	**0.51**	**0.16**

B. Comparison with state-of-the-art systems

In this section, the proposed system, referred here to as Color LADCT$_1^{HV}$+WA, is assessed in comparison with existing state-of-the- art systems, namely Basic PRNU [8], the Maximum Likelihood Estimator MLE[3] [10], Phase PRNU [11], Color Decoupling estimator (CD PRNU) [21], wavelet-based Mihcak's filter followed by Weighted Averaging (Wavelet+WA) [16], and Wiener-median PRNU [19]. The comparative analysis covers three different aspects, i.e., source camera identification, source camera verification, and the purity of PRNU estimation. It is worth mentioning that CCN has been used in the proposed system as described in subsection II-D.

1) Source camera identification: In source camera identification, the forensic analyst possesses a number of cameras and the objective is to identify the camera used to take a picture. Here, it is assumed that the picture has been taken by one of the cameras available. Therefore, a test image is assigned to a specific camera if the corresponding PRNU provides the highest similarity when compared with the noise residue extracted from that image as described earlier in section III-A. The results of FNR and FPR on our dataset and the Dresden dataset are depicted in Table VIII. As can be seen, the proposed system provides the best performance on the two datasets for all image sizes. The difference is more significant on the Dresden Dataset with clear enhancements to FPR and FNR exceeding 50% when compared with other techniques. If one takes the Basic PRNU technique [8] as a reference point, the Wiener-median PRNU technique [19] does not bring clear improvements. It is, however, worth highlighting some improvements with larger size images which suggest that the technique is sensitive to the image size.

2) Source camera verification: The task of the forensic analyst in source camera verification is to verify whether a source camera has been used to acquire a given picture. Because a threshold must be set in order to reach such a decision, one can use a range of values in order to measure the performance of the system, i.e., the False Acceptance Rate (FAR) and the True Acceptance Rate (TAR), for each threshold value as will be described later. This leads us to what is known in the literature as the Receiver Operating Characteristics (ROC) curve. Again, 50 images per camera are used to estimate the PRNU while the remaining images are used in the testing. In this experiment, 23 cameras (our dataset combined with the Dresden dataset) have been used to calculate the values of similarity between each source camera PRNU and the noise residues extracted from images of different cameras. This enables us to calculate FAR as follows. Denote by $CCN(x^j, y_i^k)$ the measure of similarity between the PRNU x^j of a camera C^j and the noise residue y_i^k of an image i taken by the camera C^k. Given M different cameras and N_j test images per camera C^j, the FAR for each threshold T can be determined as

$$\begin{aligned} FAR(T) &= Prob(CCN(x^j, y_i^k) > T | y_i^k \notin C^j) \\ &\quad (k,j) \in \{1,2,\cdots,M\} \; ; \; i \in \{1,2,\cdots,N_j\} \end{aligned} \tag{29}$$

On the other hand, the values of similarity between each source camera PRNU and the noise residues extracted from images of the same camera have been calculated and compared against the same threshold value T to determine TAR as

$$\begin{aligned} TAR(T) &= Prob(CCN(x^j, y_i^j) > T) \\ &\quad j \in \{1,2,\cdots,M\} \; ; \; i \in \{1,2,\cdots,N_j\} \end{aligned} \tag{30}$$

It is worth mentioning here that the process of removing the shared component is conducted as proposed in [10] to reduce the correlation between the PRNUs extracted from different cameras. The ROC curve performance of the proposed system along with that of existing state-of-the-art techniques are displayed in Fig. 4, 5, and 6 for various image sizes respectively.

In practical applications, it is extremely important to ensure a sufficiently low FAR (the ROC performance against low FPR is more critical); consequently, the horizontal axis of all the ROC curves is adjusted to illustrate the detail of the ROC at low FAR accordingly. The experimental results show that the proposed system performs better than its competitors. This is true for all image sizes. In Tables IX and X, the TAR at fixed values of FAR (10^{-2} and 10^{-3}) are depicted.

As can be seen, the systems perform differently in source camera verification when compared to the results of source camera identification. Indeed, the CD PRNU technique is outperformed by the basic PRNU technique. Interestingly, the Wiener-median PRNU technique appears significantly more

[3]We note that the MLE technique [10] delivered adversary results for $\sigma = 5$ as opposed to the best performance shown here with $\sigma = 3$.

TABLE VIII
OVERALL FNR AND FPR RESULTS IN (%) ON BOTH DATASETS WITH DIFFERENT TECHNIQUES.

	Our Dataset						Dresden Dataset					
	FNR			FPR			FNR			FPR		
Technique	128	256	512	128	256	512	128	256	512	128	256	512
Basic PRNU [8]	24.15	11.27	6.88	2.06	0.94	0.58	29.90	10.53	2.51	3.26	1.13	0.28
MLE [10]	23.54	11.04	6.35	1.96	0.91	0.53	28.45	10.34	2.46	3.16	1.12	0.27
Phase PRNU [11]	23.27	11.00	6.31	1.94	0.92	0.53	28.45	10.10	2.03	3.14	1.12	0.23
CD PRNU [21]	23.88	10.21	5.81	1.99	0.85	0.50	31.25	10.48	2.32	3.50	1.10	0.26
Wavelet+WA [16]	22.31	10.58	6.23	1.89	0.90	0.54	23.72	7.44	1.69	2.62	0.92	0.20
Wiener-median PRNU [19]	29.15	13.08	6.38	2.43	1.09	0.52	30.00	10.92	2.37	3.33	1.21	0.26
Color LADCT$_1^{HV}$+WA	**21.27**	**9.85**	**5.46**	**1.77**	**0.82**	**0.48**	**14.11**	**3.96**	**0.93**	**1.74**	**0.70**	**0.10**

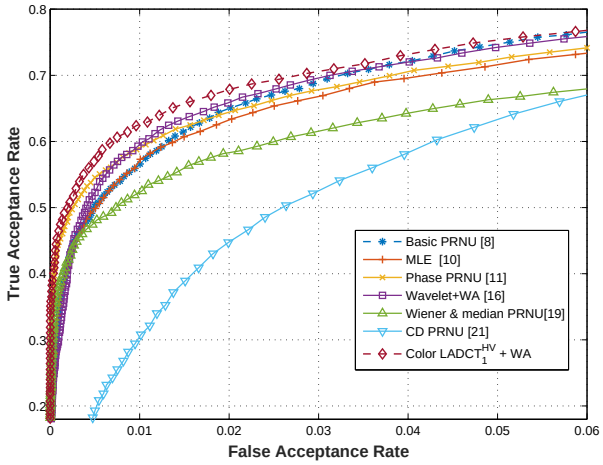

Fig. 4. Overall ROC curves with image size 128×128.

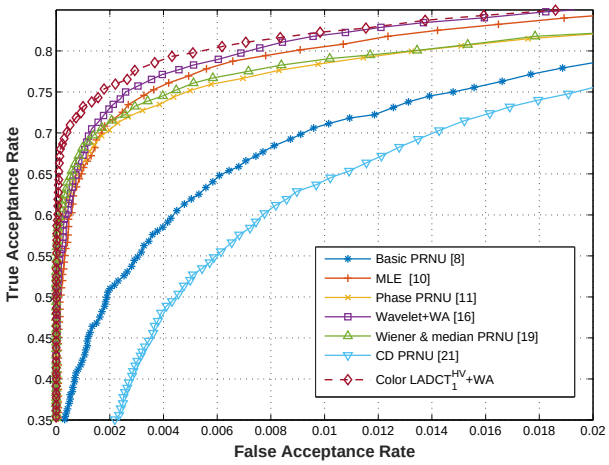

Fig. 5. Overall ROC curves with image size 256×256.

TABLE IX
TAR AT FAR=10^{-2}.

Technique	128×128	256×256	512×512
Basic PRNU [8]	0.5660	0.7113	0.7608
MLE [10]	0.5730	0.8081	0.9286
Phase PRNU [11]	0.5878	0.7839	**0.9317**
CD PRNU [21]	0.3079	0.6460	0.7392
Wavelet+WA [16]	0.5929	0.8178	0.9283
Wiener-median PRNU [19]	0.5251	0.7906	0.9214
Color LADCT$_1^{HV}$+WA	**0.6238**	**0.8227**	**0.9317**

powerful than CD PRNU and Basic PRNU on images of size 256×256 and 512×512 and close to the phase PRNU.

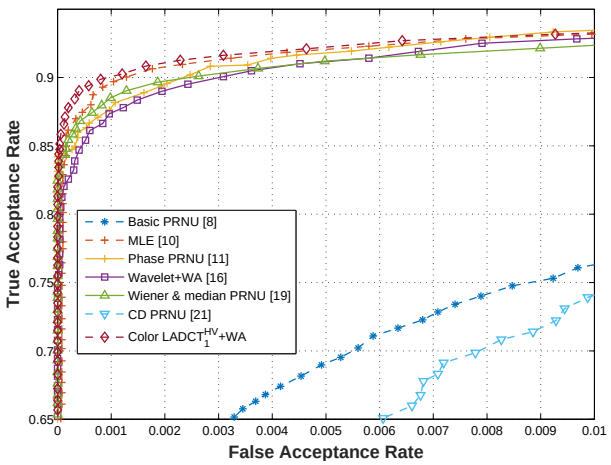

Fig. 6. Overall ROC curves with image size 512×512.

TABLE X
TAR AT FAR=10^{-3}.

Technique	128×128	256×256	512×512
Basic PRNU [8]	0.3358	0.4230	0.5289
MLE [10]	0.3527	0.6578	0.8965
Phase PRNU [11]	0.4480	0.6772	0.8970
CD PRNU [21]	0.0300	0.1480	0.3947
Wavelet+WA [16]	0.3116	0.6728	0.8734
Wiener-median PRNU [19]	0.3827	0.6820	0.8850
Color LADCT$_1^{HV}$+WA	**0.4647**	**0.7321**	**0.9026**

Surprisingly, CD PRNU performs worse than the Basic PRNU and MLE in camera verification. Note that CD PRNU has been shown in [21] to outperform MLE in a number of PRNU-based image authentication experiments but these were slightly different from ours. Indeed, in the ROC curves plotted in [21], the authors estimated the values of TAR and FAR for an individual camera by varying a certain threshold. This is a single camera verification problem and such a different setting could justify the different performance here since our varying threshold is applied to multiple cameras in order to estimate the overall TAR and FAR. In this context, it is worth noting that experiments on single and multiple camera verification were conducted by Swaminathan *et al.* in [47] where it was shown that the performance of their system differs in each experiment. Overall, the results of source camera verification confirm the superiority of the proposed system.

3) Purity of the PRNU: In this experiment, we aim to quantify the purity of the estimated PRNU with the proposed system as well as with other competing systems. The idea

underlying this experiment is that the similarity between PRNUs extracted from the same sensor must be equal to the highest possible value while the similarity between PRNU's estimated from different cameras must be minimum because the actual PRNUs are statistically independent and similar to a white Gaussian noise. Five PRNUs have been estimated for each digital camera where each uses 50 different images. Different block size values have been considered (64×64, 128×128 and 256×256). Similar to sub-section III-B2, we have combined our dataset with the Dresden dataset to obtain a consistent number of similarity measures. These measures have been collected by comparing each PRNU with all other PRNUs. The Equal Error Rate (EER) has been adopted in this experiment to illustrate the purity of PRNU estimation for each technique. The EER defines the point in percentage where the false rejection rate (i.e., $100(1 - TAR)$) becomes equal to the false acceptance rate. This can be determined by finding a threshold T^* so that $FAR(T^*) = 100(1-TAR(T^*))$. As can be seen in Table XI, the proposed system offers the smallest EER values. Interestingly, PRNU estimation with the Basic PRNU technique and MLE is less accurate than that with other competing techniques for the block size of 128×128 and 256×256. This suggests that the estimation of the noise residue from individual images plays a crucial role in source camera identification and verification.

TABLE XI
EER (%) ILLUSTRATING THE PURITY OF ESTIMATED PRNUS.

Technique	64×64	128×128	256×256
Basic PRNU [8]	2.62	2.60	2.18
MLE [10]	2.20	1.31	0.007
Phase PRNU [11]	2.54	0.87	**0**
CD PRNU [21]	3.09	0.90	**0**
Wavelet+WA [16]	2.28	1.83	**0**
Wiener-median PRNU [19]	2.64	0.95	**0**
Color LADCT$_1^{HV}$+WA	**2.17**	**0.51**	**0**

IV. CONCLUSION

In this paper, an efficient source camera identification and verification system has been introduced. The idea uses an improved locally adaptive DCT Filter followed by a weighted averaging method to exploit the content of images carrying the PRNU efficiently. Furthermore, since the physical PRNU is present in all color planes, the estimated color PRNUs have been concatenated for better matching. The system has been thoroughly assessed where the gain obtained with each of its components has been highlighted through intensive experiments on two different image datasets considering various image sizes. Finally, an experimental analysis covering three application scenarios in digital image forensics has shown the superiority of the proposed system over state-of-the-art techniques.

V. ACKNOWLEDGEMENT

This work was supported by the EPSRC Research Grant (EP/L006812/1).

APPENDIX A
PROOF OF (20)

First, to obtain an unbiased estimation, the weights are assumed to sum up to 1; that is [45]

$$\sum_{k=1}^{N} w_k = 1 \tag{31}$$

Let us define the Mean Square Error (MSE) as

$$e = \frac{1}{L}\sum_{j=1}^{L}(\hat{s}(j) - s(j))^2 \tag{32}$$

where $\hat{s}$ is the estimated version of s as given by (19). In a matrix form, the MSE can be expressed as

$$\begin{aligned} e &= E[(W^T X - s)^2] \\ &= W^T E[XX^T]W + E[s^2] - 2W^T E[sX] \end{aligned} \tag{33}$$

where T is the transpose operation. $X = [x_1, x_2, \cdots, x_N]^T$ and $W = [w_1, w_2, \cdots, w_N]^T$. The gradient of the MSE in respect to W is

$$\Delta_W(e) = 2E[XX^T]W - 2E[sX] \tag{34}$$

Minimizing the MSE leads to the following estimate

$$E[XX^T]W^* = E[sX] \tag{35}$$

Under the assumption that the noise Ψ_i is centered (i.e., zero mean) and independent of the signal s, we obtain

$$E[XX^T] = U^T E[s^2]U + \begin{pmatrix} \sigma_1^2 & 0 & \cdots & 0 \\ 0 & \sigma_2^2 & \cdots & 0 \\ \vdots & \vdots & \ddots & \vdots \\ 0 & 0 & \cdots & \sigma_N^2 \end{pmatrix} \tag{36}$$

where $U = [1, 1, \cdots, 1]$ and $E[sX] = E[s^2]U^T$. From (35) and (36), it follows

$$w_1^*\sigma_1^2 = w_2^*\sigma_2^2 = \cdots = w_N^*\sigma_N^2 \tag{37}$$

In view of (31) and (37), the weights can be deduced as

$$w_i^* = \frac{1}{\sigma_i^2}\left(\frac{1}{\sum_{k=1}^{N}\frac{1}{\sigma_k^2}}\right) \tag{38}$$

REFERENCES

[1] M. Zimba and S. Xingming, "DWT-PCA(EVD) based copy-move image forgery detection," *International Journal of Digital Content Technology and its Applications*, vol. 5, pp. 251–258, Jan. 2011.
[2] A. C. Popescu and H. Farid, "Exposing digital forgeries in color filter array interpolated images," *IEEE Transactions on Signal Processing*, vol. 53, pp. 3948–3959, Oct. 2005.
[3] A. Swaminathan, M. Wu, and K. Liu, "Nonintrusive component forensics of visual sensors using output images," *IEEE Transactions on Information Forensics and Security*, vol. 2, pp. 91–106, Mar. 2007.
[4] K. San Choi, E. Y. Lam, and K. K. Wong, "Source camera identification using footprints from lens aberration," in *Proc. SPIE Digital Photography II*, San Jose, CA, Jan. 2006, p. 60690J.
[5] L. T. Van, S. Emmanuel, and M. S. Kankanhalli, "Identifying source cell phone using chromatic aberration," in *Proc. IEEE International Conference on Multimedia and Expo*, Beijin, Jul. 2007, pp. 883–886.
[6] A. E. Dirik, H. T. Sencar, and N. Memon, "Digital single lens reflex camera identification from traces of sensor dust," *IEEE Transactions on Information Forensics and Security*, vol. 3, pp. 539–552, Aug. 2008.

[7] J. Lukas, J. Fridrich, and M. Goljan, "Digital bullet scratches for images," in *Proc. IEEE International Conference on Image Processing (ICIP)*, Genova, Italy, Sep. 2005, pp. III–65–8.

[8] J. Lukas, J. Fridrich, and M. Goljan, "Digital camera identification from sensor pattern noise," *IEEE Transactions on Information Forensics and Security*, vol. 1, pp. 205–214, Jun. 2006.

[9] M. Chen, J. Fridrich, and M. Goljan, "Digital imaging sensor identification (further study)," in *Proc. SPIE Electronic Imaging*, CA, USA, Jan. 2007, pp. 0P–0Q.

[10] M. Chen, J. Fridrich, M. Goljan, and J. Lukas, "Determining image origin and integrity using sensor noise," *IEEE Transactions on Information Forensics and Security*, vol. 3, pp. 74–90, Mar. 2008.

[11] X. Kang, Y. Li, Z. Qu, and J. Huang, "Enhancing source camera identification performance with a camera reference phase sensor pattern noise," *IEEE Transactions on Information Forensics and Security*, vol. 7, pp. 393–402, Apr. 2012.

[12] C.-T. Li, "Source camera identification using enhanced sensor pattern noise," *IEEE Transactions on Information Forensics and Security*, vol. 5, pp. 280–287, Jun. 2010.

[13] A. Lawgaly, F. Khelifi, and A. Bouridane, "Image sharpening for efficient source camera identification based on sensor pattern noise estimation," in *Proc. International Conference on Emerging Security Technologies*, Cambridge, UK, Sep. 2013, pp. 113–116.

[14] Y. Hu, B. Yu, , and C. Jian, "Source camera identification using large components of sensor pattern noise," in *Proc. International Conference on Computer Science and its applications*, Seoul, Korea, Jul. 2009, pp. 1–5.

[15] Y. Tomioka, Y. Ito, and H. Kitazawa, "Robust digital camera identification based on pairwise magnitude relations of clustered sensor pattern noise," *IEEE Transactions on Information Forensics and Security*, vol. 8, pp. 1986–1995, Dec. 2013.

[16] A. Lawgaly, F. Khelifi, and A. Bouridane, "Weighted averaging-based sensor pattern noise estimation for source camera identification," in *Proc. IEEE International Conference on Image Processing (ICIP)*, Paris, France, Oct. 2014, pp. 5357–5361.

[17] R. Li, Y. Guan, and C.-T. Li, "PCA-based denoising of sensor pattern noise for source camera identification," in *Proc. IEEE China Summit and International Conference on Signal and Information Processing (ChinaSIP)*, China, Jul. 2014, pp. 436–440.

[18] D. Valsesia G. Coluccia T. Bianchi and E. Magli, "Compressed fingerprint matching and camera identification via random projections," *IEEE Transactions on Information Forensics and Security*, vol. 10, pp. 1472–1485, Jul. 2015.

[19] A. J. Cooper, "Improved photo response non-uniformity (PRNU) based source camera identification," *Forensic science international*, vol. 226, pp. 132–141, 2013.

[20] X. Kang, J. Chen, K. Lin, and P. Anjie, "A context-adaptive SPN predictor for trustworthy source camera identification," *EURASIP Journal on Image and Video Processing*, vol. 2014, pp. 1–11, Apr. 2014.

[21] C.-T Li and Y. Li, "Color-decoupled photo response non-uniformity for digital image forensics," *IEEE Transactions on Circuits and Systems for Video Technology*, vol. 22, pp. 260–271, Feb. 2012.

[22] Y. Hu, C.-T. Li, and C. Jian, "Building fingerprints with information from three color bands for source camera identification," in *Proc. ACM workshop on Multimedia in forensics, security and intelligence*, Firenze, Italy, Oct. 2010, pp. 111–116.

[23] M. Goljan, J. Fridrich, and T. Filler, "Large scale test of sensor fingerprint camera identification," in *Proc. SPIE Electronic Imaging*, CA, USA, Jan. 2009, p. 72540I.

[24] X. Lin and C.-T. Li, "Preprocessing reference sensor pattern noise via spectrum equalization," *IEEE Transactions on Information Forensics and Security*, vol. 11, pp. 126–140, Jan. 2016.

[25] S. Chenyang, S. Yuting, Z. Jing, and X. Junyu, "Sensor pattern noise in JPEG compressed images," in *Proc. International Conference on Audio, Language and Image Processing (ICALIP)*, Shanghai, China, Jul. 2012, pp. 155–159.

[26] M. Goljan, J. Fridrich, and J. Lukas, "Camera identification from printed images," in *Proc. SPIE Electronic Imaging*, CA, USA, Jan. 2008, p. 68190I.

[27] Z. Qu, X. Kang, J. Huang, and Y. Li, "Forensic sensor pattern noise extraction from large image data set," in *Proc. IEEE International Conference on Acoustics, Speech and Signal Processing (ICASSP)*, Vancouver, Canada, May. 2013, pp. 3023–3027.

[28] J. R. Janesick, *Scientific charge-coupled devices*, SPIE Press, 2001.

[29] G. Chierchia, S. Parrilli, G. Poggi, C. Sansone, and L. Verdoliva, "On the influence of denoising in prnu based forgery detection," in *Proc. of the 2Nd ACM Workshop on Multimedia in Forensics, Security and Intelligence*, Firenze, Italy, Oct. 2010, pp. 117–122.

[30] A. Cortiana, V. Conotter, G. Boato, and F. G. B. De Natale, "Performance comparison of denoising filters for source camera identification," in *Proc. SPIE Conference on Media Watermarking, Security, and Forensics*, CA, USA, Jan. 2011, p. 788007.

[31] K. Dabov, A. Foi, V. Katkovnik, and K. Egiazarian, "Image denoising by sparse 3-D transform-domain collaborative filtering," *IEEE Transactions on Image Processing*, vol. 16, pp. 2080–2095, Aug. 2007.

[32] M. K. Mihcak, I. Kozintsev, and K. Ramchandran, "Spatially adaptive statistical modeling of wavelet image coefficients and its application to denoising," in *Proc. IEEE International Conference on Acoustics, Speech, and Signal Processing (ICASSP)*, Arizona, USA, Mar. 1999, vol. 6, pp. 3253–3256.

[33] X. Lin and C.-T. Li, "Enhancing sensor pattern noise via filtering distortion removal," *IEEE Signal Processing Letters*, vol. 23, no. 3, pp. 381–385, Mar. 2016.

[34] M. Goljan, *Digital Watermarking*, chapter Digital camera identification from images-Estimating false acceptance probability, pp. 454–468, Lecture notes in Computer Science. Springer, 2009.

[35] J.-U. Hou and H. K. Lee, "Detection of hue modification using photo response non-uniformity," *To appear in IEEE Transactions on Circuits and Systems for Video Technology*, 2016, DOI:10.1109/TCSVT.2016.2539828.

[36] D. Kurkin, V. Lukin, V. Abramova, S. Abramov, B. Vozel, and K. Chehdi, "Image DCT coefficient statistics and their use in blind noise variance estimation," in *Proc. International Conference on Mathematical Methods in Electromagnetic Theory (MMET)*, Kharkiv, Ukraine, Aug. 2012, pp. 316–319.

[37] R. Oktem, K. Egiazarian, V. V. Lukin, N. N. Ponomarenko, and O. V. Tsymbal, "Locally adaptive DCT filtering for signal-dependent noise removal," *EURASIP Journal on Advances in Signal Processing*, vol. 2007, pp. 1–10, 2007, Article ID 42472.

[38] N. N. Ponomarenko, V. V. Lukin, A. A. Zelensky, J. T. Astola, and K. O. Egiazarian, "Adaptive DCT-based filtering of images corrupted by spatially correlated noise," in *Proc. SPIE Electronic Imaging*, CA, USA, Jan. 2008, p. 68120W.

[39] V. V. Lukin, D. V. Fevralev, N. N. Ponomarenko, S. K. Abramov, O. Pogrebnyak, K. O. Egiazarian, and J. T. Astola, "Discrete cosine transform-based local adaptive filtering of images corrupted by nonstationary noise," *Journal of Electronic Imaging*, vol. 19, pp. 023007, May 2010.

[40] R. R. Coifman and D. L. Donoho, *Translation-invariant de-noising*, Springer, 1995.

[41] D. L. Donoho, "De-noising by soft-thresholding," *IEEE Transactions on Information Theory*, vol. 41, pp. 613–627, Mar. 1995.

[42] E. Laciar and R. Jane, "An improved weighted signal averaging method for high-resolution ECG signals," in *Proc. Computers in Cardiology*, Rotterdam, Holland, Sep. 2001, pp. 69–72.

[43] A. Momot, *Applied Biomedical Engineering*, chapter 16. Methods of Weighted Averaging with Application to Biomedical Signals, pp. 361–386, Edited by G. D. Gargiulo and A. McEwan, INTECH Open Access Publisher, 2011.

[44] W. V. Drongelen, *Signal processing for neuroscientists: an introduction to the analysis of physiological signals*, Academic Press, 2006.

[45] E. Bataillou, E. Thierry, H. Rix, and O. Meste, "Weighted averaging using adaptive estimation of the weights," *Signal Processing*, vol. 44, pp. 51–66, Jun. 1995.

[46] T. Gloe and R. Bohme, "The dresden image database for benchmarking digital image forensics," *Journal of Digital Forensic Practice*, vol. 3, pp. 150–159, 2010.

[47] A. Swaminathan, M. Wu, and K. J. R. Liu, "Digital image forensics via intrinsic fingerprints," *IEEE Transactions on Information Forensics and Security*, vol. 3, pp. 101–117, Mar. 2008.